Preprint. J. E. Shepherd. Detonation in gases. In Proceedings of the Combustion Institute, Volume 32, pages 83-98, 2009. http://dx.doi.org/10.1016/j.proci.2008.08.006

Detonation in Gases

J.E. Shepherd

Aeronautics and Mechanical Engineering
California Institute of Technology,
Pasadena, California 91125, USA

Abstract

We review recent progress in gaseous detonation experiment, modeling, and simulation. We focus on the propagating detonation wave as a fundamental combustion process. The picture that is emerging is that although all propagating detonations are unstable, there is a wide range of behavior with one extreme being nearly laminar but unsteady periodic flow and the other chaotic instability with highly turbulent flow. We discuss the implications of this for detonation propagation and dynamic behavior such as diffraction, initiation, and quenching or failure.

Key words: Detonation, reaction zone structure, transverse waves, instability, turbulence
PACS: 47.70.Pq, 47.40.Rs, 82.33.Vx

Email address: joseph.e.shepherd@caltech.edu (J.E. Shepherd).
URL: http://www.galcit.caltech.edu/~jeshep/ (J.E. Shepherd).

1 Introduction

Fill a long tube with a fuel–oxygen mixture, ignite it with a spark at one end, and you are likely to observe a supersonic combustion wave or detonation moving with a remarkably constant speed that is between five and ten times the velocity of sound in the original mixture. The combustion products are set into motion behind the front, and an expansion wave brings the gas back to rest, creating the traveling pressure wave shown in Fig. 1a. Following the discovery of this phenomenon by Berthelot and Vielle [1] and Mallard and Le Chatelier [2] in 1881, this has been a source of fascination and investigation by scientists and engineers. The possibility of using the force on the tube for propulsion [3,4] has motivated many recent studies of detonation. Another motivation is industrial safety since the forces created by the detonation can cause mechanical failure of pressure vessels and pipelines [5,6], particularly when a detonation is formed following the acceleration of a flame within a duct or pipe [7].

One of the earliest successes in combustion science was the Chapman and Jouguet (CJ) model to predict the detonation speed based solely on conservation laws and thermodynamic properties [8]. Once the detonation velocity is known, the mean flow of the following gas can be completely determined without any consideration of the front. The computed flow is in remarkable agreement with measurements of velocity, pressure, OH concentration, and temperature [9,10] if the effects of friction and heat transfer are included [11]. The success of the CJ model for ideal detonations is associated with the existence of a sonic surface behind the front [12,13] that isolates the front from disturbances from the rear. The wave speed is determined by the extent of reaction before the sonic surface is reached, and for ideal waves, the reaction is essentially complete at this point so that the wave speed is independent of chemical reaction kinetics. This *hydrodynamic* approach is adequate for most engineering purposes, but the chemical reaction kinetics must be considered to understand dynamic events like initiation, quenching, and diffraction.

Chemical reaction takes place at the head of the detonation wave where a shock wave is followed by a thin reaction zone (less than 1 mm for fuel–oxygen mixtures at high pressure) which appears as a thin bright line on a high-speed chemiluminescence image or a nearly planar density jump in a schlieren or shadow image, Fig. 1b. Although the front (vertical dark line) appears remarkably flat in this image, the flow is clearly nonuniform behind the front with a series of periodic striations extending horizontally to the rear of the main flow. Discovered in the late 1950s [14,15] and extensively studied in the 1960s [16–21] (see the full history in Chap. 6 of Lee [22]), these are shock waves moving transversely (perpendicular) to the main front and are evidence of the ubiquitous instability of detonation fronts. Although these waves appear

to be weak disturbances on a primarily one-dimensional flow, they can have a profound effect on the detonation wave behavior, intriguing and perplexing researchers for the last 50 years.

If we neglect the effect of the transverse waves, we can apply the ideal reaction zone theory of Zeldovich [23], Doering [24], and von Neumann [25] (ZND) to compute the flow within the reaction zone. The ZND model supposes a steadily-moving shock wave (the jump in pressure and temperature at $x = 0$ in Fig. 1c) followed by reaction in a constant-area, inviscid, compressible flow. The temperature rises and pressure drops in Fig. 1c as the reactants are converted to intermediates and finally to products in Fig. 1d.

In this ideal model, the coupling from the chemistry to the fluid mechanics occurs primarily through the thermicity $\dot{\sigma}$ (see Chaps. 4 and 5 of [26]), which can be visualized as a pulse of energy deposited into the flow some distance behind the shock front as shown in Fig. 1c. The coupling from the fluid mechanics to the chemistry occurs through the dependence of reaction rates on the species concentrations, pressure, and temperature. The pulse width ($\Delta_e = 0.1$ mm in Fig. 1c) and the distance to the peak energy release ($\Delta_i = 0.2$ mm in Fig. 1c) are determined by the chemical reaction mechanism, rates of reaction, and the thermodynamic state behind the shock front.

Most importantly, the ideal steady structure is unstable [27] with respect to small disturbances in lead shock shape and speed. The linear instability is a consequence of the amplification of acoustic waves that are trapped in the acoustic resonator composed of the region between the lead shock and the end of the energy release zone ($0 < x < 0.3$ mm in Fig. 1c), the sensitivity of the chemical reaction rates to the thermodynamic state (temperature and pressure) behind the shock front, and the hydrodynamic instability of propagating reaction fronts. The growth rates of the linear instability are sufficiently large that laboratory observations of propagating detonations are almost exclusively of "multi-front" waves [28] with large-amplitude (nonlinear), three-dimensional wavefront perturbations and associated transverse waves. The nonlinear perturbations result in a reaction zone that is spatially nonuniform and unsteady but presumed to be statistically stationary with an average propagation speed that is close to the CJ value.

For the remainder of this review, we will focus on the characterization of the detonation front and the implications for detonation behavior. Knowledge of the mechanisms of ignition and combustion within the front are central to improving our understanding of detonation waves. We describe advances made through experiments and numerical simulations that resolve the nonsteady and turbulent structure of the reaction zone. For a fuller account of this and all other aspects of gaseous detonations, see the comprehensive monograph by Lee [22].

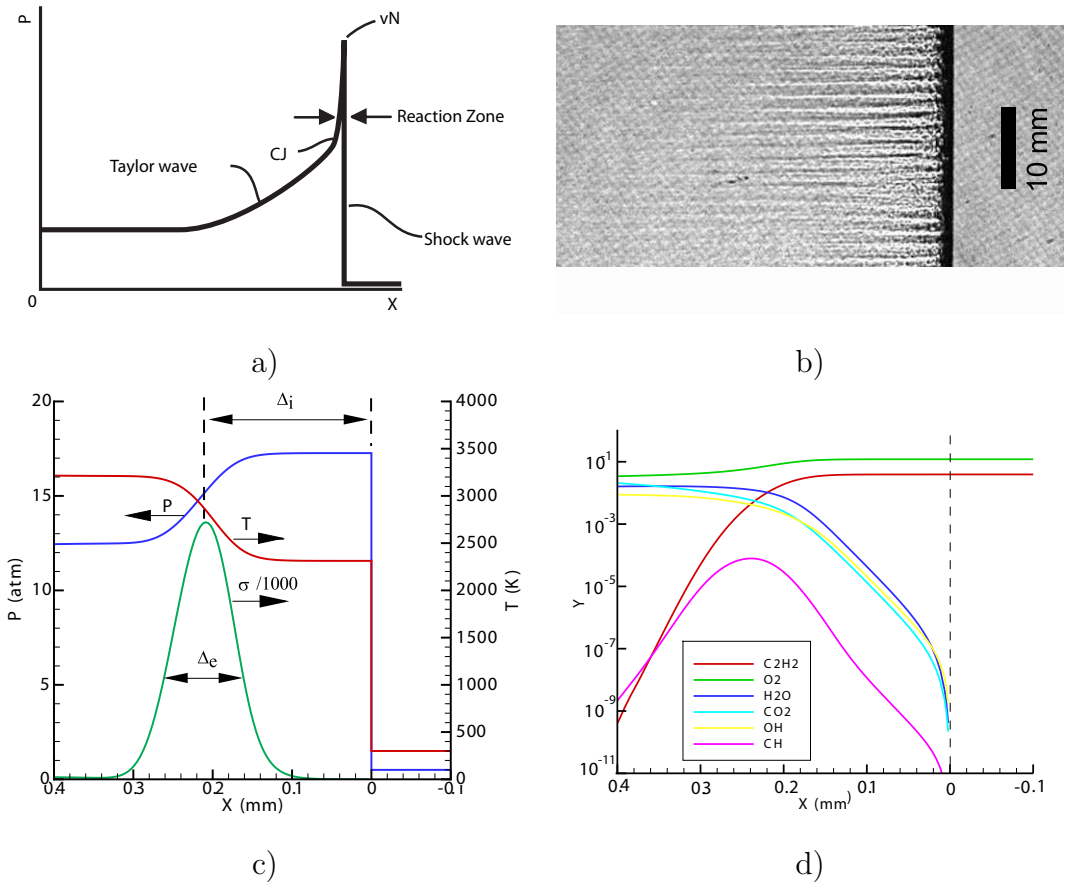

Fig. 1. Detonation front propagating from left to right in C_2H_2+3O_2+14Ar. a) Profile produced by fluid motion [29,30] behind an ideal detonation started at the closed end of a tube. b) Schlieren image of reaction front [31]. c) Ideal reaction zone (ZND) profile of pressure, temperature, and thermicity. d) Ideal reaction zone (ZND) profile of species mass fractions.

2 Visualizing Detonation Fronts

The ideal reaction zone in Figs. 1c and d occurs in a spatial region less than the width of the dark vertical line in Fig. 1b that represents the density gradient due to the shock and reaction zone combined. In order to visualize the processes within the reaction zone, either very high magnification is needed in the optical system or the mixture parameters must be chosen to increase the reaction zone width. Lowering the pressure or adding an inert gas like nitrogen will decrease the postshock temperature and increase the characteristic reaction zone thickness.

Austin [32] investigated the reaction zone of a range of mixtures at initial pressures between 7 and 30 kPa. Additionally, instead of the rectangular 150 × 150 mm section used to record Fig. 1b, she used an 18 × 150 mm channel to create an approximately two-dimensional flow to obtain the schlieren images

shown in Fig. 2. The light source [31] for the images is a Q-switched ruby laser with a pulse width of 50 ns in order to minimize the motion blur. With this approach, the leading shock front, transverse waves, and fine-scale turbulence within the reaction zone can now all be clearly observed. The detonation channel is about three meters long and a special initiation system [33] was used to start the detonations with a planar front and ensure a rapid establishment of a steadily propagating wave.

The schlieren images in Fig. 2 now clearly show the curvature of the leading shock front and the discontinuity in curvature at the intersections or triple points between the transverse waves and main shock front. There are striking qualitative differences [34–36] between the argon-diluted mixtures (a and b) and the nitrogen-diluted mixtures (c and d). Mixtures a and b have smooth fronts away from the triple points, very little evidence of turbulence in the reaction zone, and periodically-spaced transverse shock waves. Mixtures c and d have a rough appearance to the fronts, prominent turbulence structure within the reaction zone, and an irregular spacing of the transverse waves.

Alongside each schlieren image a photograph is shown of a soot foil , an aluminum sheet that was covered with soot and then placed on the side of the detonation channel just downstream of the observation window. This technique was first used to discover detonation instability [15] and Oppenheim [21] demonstrated the coincidence of the soot tracks with motion of triple points along the front by combining the soot track and laser schlieren method. The patterns observed on the soot foils are periodic cells with a single transverse spatial wavelength of $\lambda = 70$ mm in Fig. 2a, a less periodic but still regular pattern with a wavelength of 35–45 mm in Fig. 2b, and very irregular patterns in Figs. 2c and d with a range of spatial wavelengths between 5–32 mm for Figs. 2c and 2–52 mm for Figs. 2d.

2.1 Detonation Length Scales

The characteristic spatial wavelength observed in the soot foil patterns is conventionally termed the *detonation cell size*, usually measured as the distance λ between parallel soot tracks as shown on Fig. 2a. This is found to be empirically correlated to other length scales [37,38] that can be defined for detonation diffraction [39], initiation [40], and transition from deflagration-to-detonation [41]. Cell sizes are known for a wide range of mixtures [42], and explosion hazard evaluations and technology development programs motivate new studies [43–45]. The cell size and other length scales are strongly correlated with the ideal reaction zone length [46], and estimation of cell size based on detailed reaction mechanisms is an important tool for safety evaluations [47–51].

-

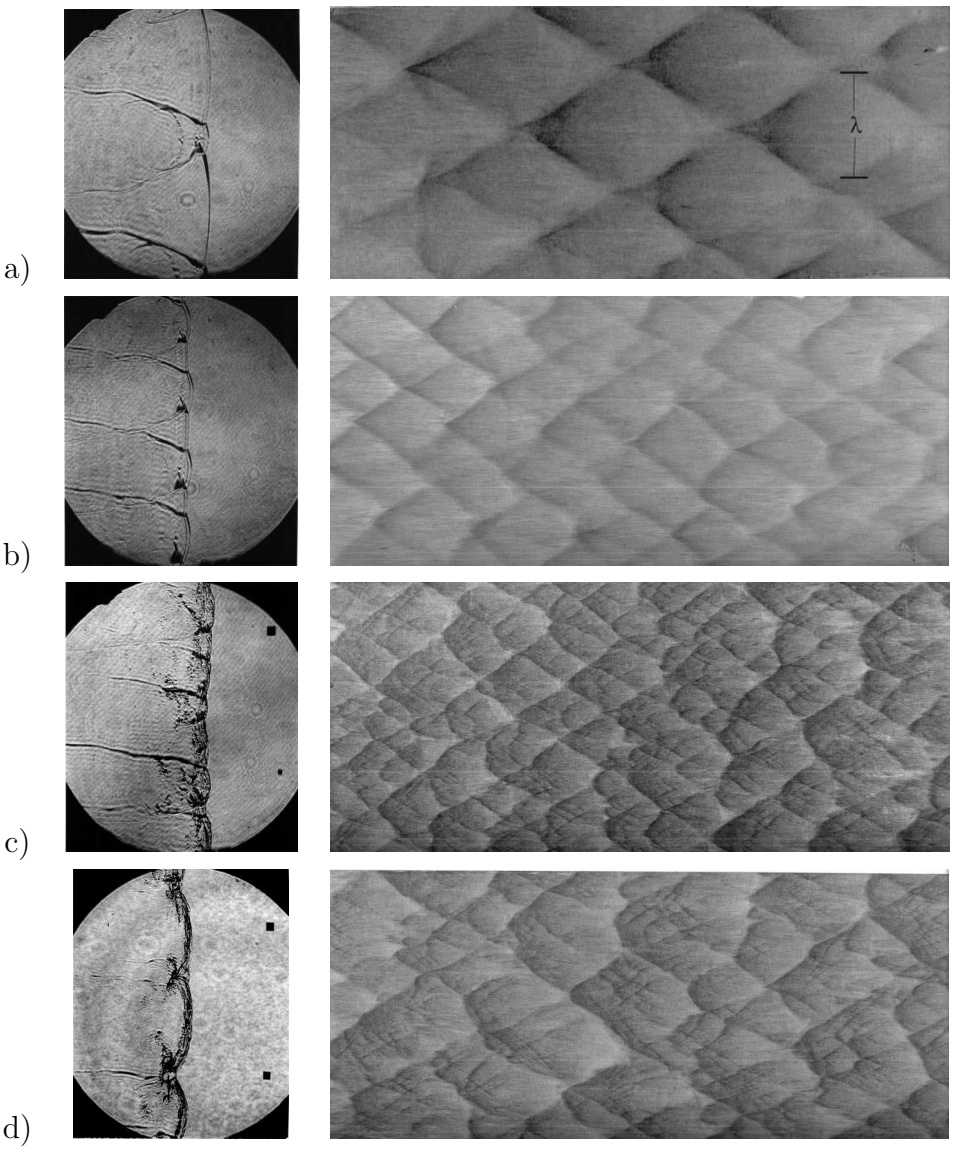

Fig. 2. Schlieren images and corresponding soot foil records at the same scale (150 mm high) and initial pressure of 20 kPa [32]. The detonations moving from left to right in this and subsequent figures. a.) $2H_2+O_2+17Ar$. b) $2H_2+O_2+12Ar$. c) $H_2+N_2O+1.33N_2$. d) $C_3H_8+5O_2+9N_2$.

Unfortunately, it is clear from Fig. 2 that the cell size is not a single well-defined quantity for irregular mixtures and if there are multiple peaks [52] in $\dot{\sigma}$, there are at least two distinct cell sizes. Image processing and statistical analysis have been proposed [53,54] in order to make cell size a more quantitative concept but these have not found widespread use. The value of cell size measurements is ultimately limited due to the lack of precision (a range of 50%–100% is not uncommon) and the vague relationship between the soot tracks and physical processes in the detonation front. However, soot foils are so simple to use that they are employed as a diagnostic in both simulations

(almost all two-dimensional simulations report "soot" tracks based on peak pressure, temperature, or reaction rate) and many experiments [55–64].

2.2 Imaging Chemistry

Soot foils, pressure traces, schlieren, streak, and open shutter imaging techniques have been used very effectively by past researchers to build our present knowledge of detonations. However, these measurements are primarily mechanical and made at the boundaries of the flow or integrated through the flow field. In order to move to the next level of understanding for detonations, we need information about the spatial and temporal variation of the chemical species, thermodynamic state, and fluid motion within the reaction zone. To do this, Pintgen developed [65,66] a planar laser-induced fluorescence (PLIF) method to obtain snapshots of the OH species concentration [OH] within the detonation reaction zone.

The idea is quite simple in concept: a pulsed laser (duration < 20 ns) is used to generate a thin (0.3 mm) sheet of UV light about 80 mm high with a wavelength in the vicinity of 284 nm. The light sheet is timed to pass perpendicularly through the detonation from the upstream region, and the stimulated emission from transitions near 315 nm is captured at approximately 90° on an intensified camera. In practice, the method requires substantial care in execution [66] and special considerations for detonation applications since the signal-to-noise ratio is modest, there is substantial background noise from chemiluminescence in the hot flow, and precise timing is needed for the illumination, detonation, and camera shuttering. In order to effectively interpret the PLIF images, we have found that it is necessary to simultaneously take a schlieren image in order to determine the location of the shock front and transverse waves relative to the OH PLIF region. The boxed region in the center of Fig. 3a was imaged by the PLIF method. An image of the induced OH emission is shown in Fig. 3b and a false-color image overlaid onto the schlieren image in Fig. 3c.

Examining Fig. 3b, as we follow the mean streamlines on a horizontal path from right to left at a fixed vertical location, the OH PLIF signal rises sharply to a maximum value and then decays slowly. The key features we observe in Fig. 3c are shown schematically in Fig. 4a. The OH PLIF signal appears to form a distinct front which is close to faster portions of the lead shock and lies further behind the slower portion of the lead shock. The interpretation of these images can be made by locally applying the ideal detonation model to a portion of the wavefront. Applying the ZND model to an unsteady wave may seem a rather crude approximation, but as discussed in Pintgen et al. [35] and described below, weakly unstable waves have quasi-steady reaction zones.

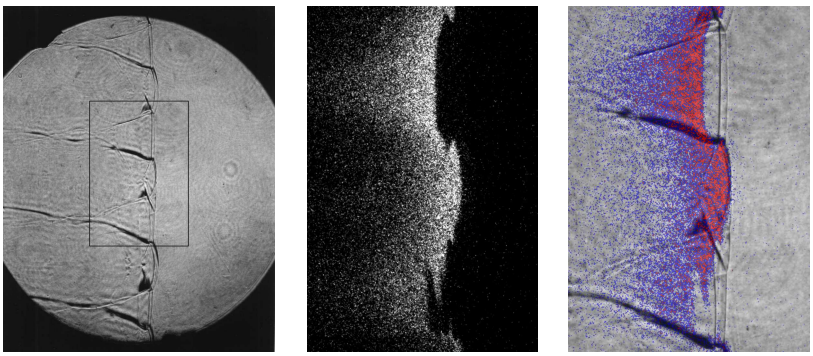

a) b) c)

Fig. 3. Visualization of detonation front in the narrow channel using combined schlieren and PLIF technique for $2H_2+O_2+12Ar$ at 20 kPa [32]. a) Laser schlieren image. b) PLIF image. c) overlay of PLIF and laser schlieren.

The ZND model structure of the reaction zone was used to predict [OH] in Fig. 4b and detailed models of the optical system, molecular collisions, light absorption and emission processes [66] have been used to predict the PLIF intensity. The sudden rise in [OH] that leads to the front-like appearance in Fig. 3b is correctly predicted, and by including the absorption of the laser sheet, the rapid decrease in the tail is also reproduced. The oscillation of the shock front (exchange of the "fast" and "slow" portions of the wave front in Fig. 4a) causes a variation in the equivalent steady wave thickness as shown in Fig. 4c. This variation is due to the Arrhenius dependence of the reaction rates on temperature and the shock jump conditions that determine postshock conditions from shock speed. In weakly unstable mixtures, the typical range of shock speed oscillation ($0.85 < U/U_{\mathrm{CJ}} < 1.25$) results in an order of magnitude change in reaction zone thickness, and more significantly, the change occurs sufficiently slower [35] that the reaction always goes to completion within 2–3 steady-state reaction zone lengths. The characteristic "keystone" shape of the OH front can be explained [32,35] by considering the quasi-steady reaction process in the triple-point region.

Although the spatial distribution of the computed PLIF intensity matches the experimental observations [66], the peak OH concentration cannot be quantitatively determined since the LIF is in the linear regime and the quenching rate must be extrapolated from low pressure data and models of the molecular collision processes. It is also important to keep in mind when interpreting the images that the light sheet has a finite thickness (0.3 mm) and the camera resolution is limited by the modest number of pixel elements in the charge-coupled device and use of the intensifier. This limits the smallest scales that we are able to observe.

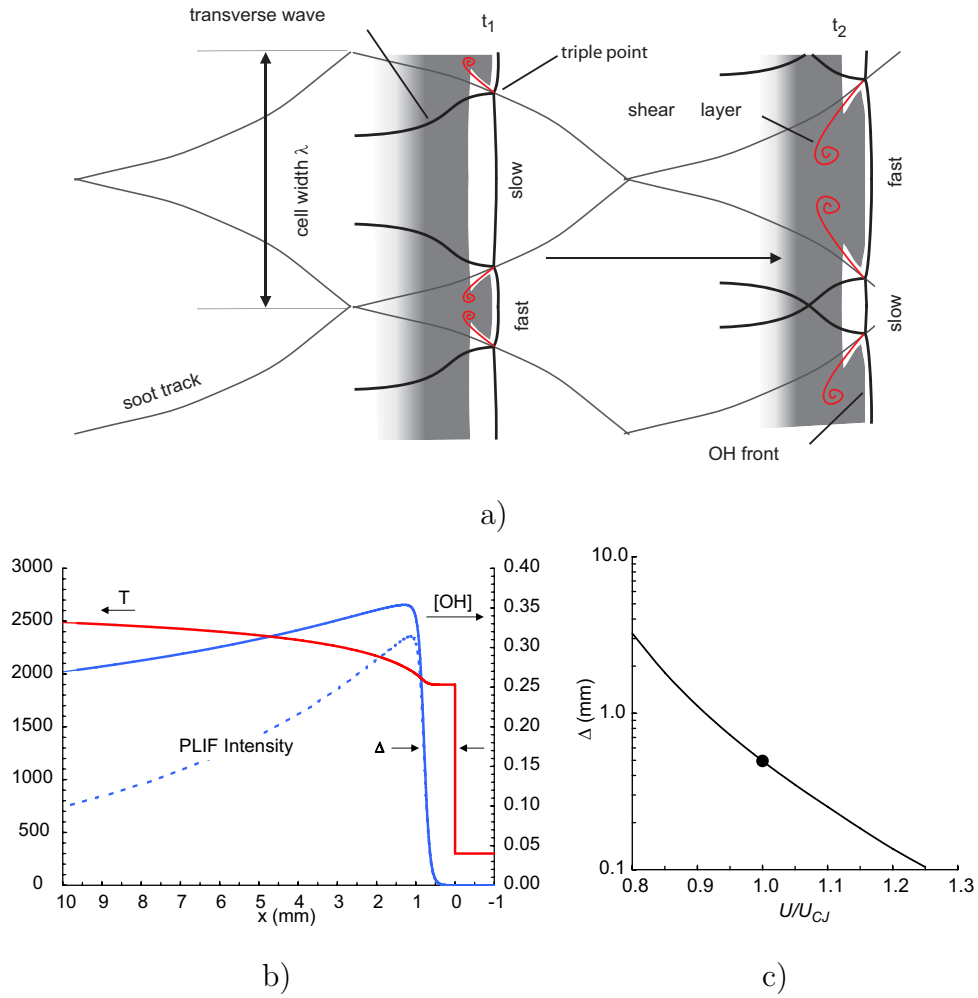

Fig. 4. a) Interpretation of weakly unstable detonation wave front PLIF and schlieren images. Computed reaction zone properties correspond to conditions of Fig. 3. b) ZND structure showing simulated PLIF intensity corrected for absorption. c) Reaction zone thickness variation with shock speed.

2.3 Highly-unstable detonations

The features observed in Fig. 3 and the interpretation given in Fig. 4 were known from previous observations based on schlieren images and soot foils [16,67–70]. However, much less is known about the details of highly-unstable detonations. The PLIF technique was applied by Austin [32] to the structure of highly-unstable reaction zones associated with irregular cellular structure. By varying the mixture composition, she was able to deliberately adjust the extent of irregularity in the cellular structure. The main guides to selecting mixtures were the experimental observations [71–73] on various mixtures and the conclusions of linear stability theory [74,75] regarding the role of effective activation energy in detonation instability.

The effective activation energy can be defined in terms of the variation of the induction length Δ_i with postshock temperature; this is closely related to the logarithmic slope of the relationship shown in Fig. 4c. The higher the reduced effective activation energy E/RT_{vN}, (T_{vN} is the postshock temperature), the more unstable the mixture. However, reduced activation energy alone is not adequate to explain the stability properties of detonations. Strehlow [71] found that experimental soot foil patterns were correlated not only with induction length and activation energy but also with the shape and other characteristics of the ZND structure. Howe et al. [76] found that shortening the energy release zone relative to the induction zone caused a greater tendency to instability in numerical simulations of detonation in one-dimension. Shepherd et al. [53] examined the role of endothermic processes and showed that some observations on instability [77] could be correlated with the limiting overdrive for creating a net thermally neutral reaction zone.

Short [78] and Short and Sharpe [79] demonstrated that a bifurcation boundary between stable and unstable detonations in one-dimension occurs when the ratio of induction to energy release length is on the order of the activation energy for a three-step model of branching-chain chemical reaction. Ng et al. [80,81] used numerical simulation of one-dimensional detonation propagation to show the broad applicability of this notion to a variety of mixtures using realistic reaction mechanisms. They found that the stability boundary was correlated with a figure of merit χ obtained by multiplying the reduced activation energy by the ratio of the induction length to the energy release pulse width (width of $\dot{\sigma}$ in Fig. 1), Δ_i/Δ_e. For the weakly unstable mixture shown in Fig. 3, Δ_i/Δ_e is approximately one, but values as high as ten are observed in the mixtures we have studied. For the highly-unstable CH_4+$2O_2$ mixture examined by Radulescu et al. [82,83], $\Delta_i/\Delta_e \sim 20$, and for stoichiometric methane–air mixture, $\Delta_i/\Delta_e \sim 60$ [80].

A selection of PLIF images from mixtures with varying degrees of instability is shown in Fig. 5. Figures 5a–c represents moderately unstable mixtures. Large-scale structures characteristic of Kelvin–Helmholtz instability are visible when the shear layer occurs between reacted and unreacted gas [34]. Pockets of low fluorescence are found within the high intensity region behind the main reaction front and in some cases, further downstream. The reaction front is distorted over a wide range of scales and quantitative geometric analysis [84] indicates that it has the character of a scale-dependent fractal. Velocity and density fluctuations appear to occur on a scale much smaller than that of the dominant cell size.

Figures 5d–f represents highly-unstable mixtures. The reaction front is very irregular and a large range of fluctuation length scales are visible. Substantial regions of low OH concentration appear near the end of the cell cycle, suggesting that the reaction rates are very low due to the effects of unsteadiness

and the low value of the leading shock velocity at these times. Bright spots, regions of high OH concentration, are observed close to the regions where transverse waves interact. High-speed camera records [36] indicate explosive events taking place at these locations. The front appears rough and wrinkled and the keystone features are less pronounced compared to weakly unstable waves [32]. Austin et al. [36,85] propose that these effects are a manifestation of the extreme sensitivity of these reaction zones to unsteadiness. They show that the fluctuations in lead shock strength for highly-unstable detonations not only result in a much larger range of scales but also much larger critical decay times [86] so that the reaction zone essentially decouples from the shock front as the main shock velocity drops slightly below the CJ value.

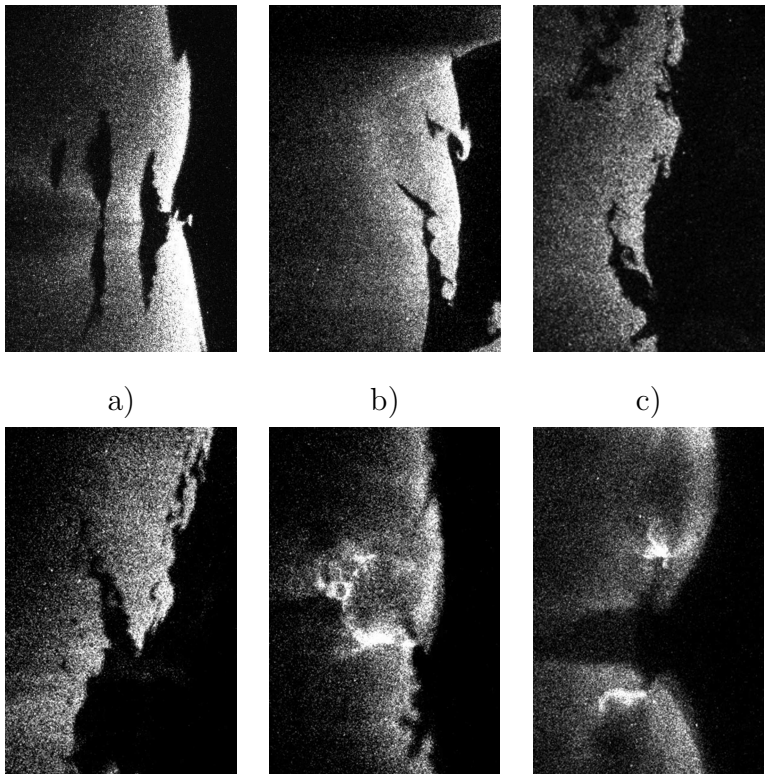

Fig. 5. PLIF images of detonation fronts with a range of unstable behavior [32,66]. a) $2H_2+O_2+3N_2$, $E/RT_{vN} = 6$, $\Delta_i/\Delta_e = 3.4$. b) $2.44H_2+O_2+8.1N_2$, $E/RT_{vN} = 7$, $\Delta_i/\Delta_e = 4.6$. c) $2H_2+N_2O+3N2$, $E/RT_{vN} = 8$–9, $\Delta_i/\Delta_e = 7.3$. d) $C_2H_4+3O_2+10.5O_2$, $E/RT_{vN} = 11$–12, $\Delta_i/\Delta_e = 2.7$. e) and f) $C_3H_8+5O_2+9N_2$, $E/RT_{vN} = 11$–13, $\Delta_i/\Delta_e = 9.7$.

2.4 Macroscopic Behavior and Mixture Type

The regular cellular patterns (Figs. 2a and b) are associated with "weakly unstable" fronts [35] with only a single transverse wavelength and smooth

wavefronts. The irregular cellular patterns (Figs. 2c and d) are associated with "strongly unstable" fronts [36] with a large spectrum of transverse wavelengths and fine-scale wrinkling on the shock and OH fronts. The macroscopic behavior, such as initiation, diffraction, and quenching events, that occurs over distances that are $> 10^3\ \Delta_i$ is observed to be quantitatively different for these two types of mixtures. These differences suggest that the microscopic behavior within the front creates a fundamentally different feedback mechanism between fluid dynamics and overall energy release for the two extremes of weakly and strongly unstable waves.

The first evidence for the macroscopic difference in mixture types was put forward by Subbotin [70], who examined the two mixture types and concluded that in weakly unstable waves the reaction took place behind the transverse waves and no unburned pockets were formed. For strongly unstable waves, the transverse waves were unreactive and irregular pockets of unburned gas were observed downstream of the front. However, if the mean detonation speed was sufficiently low, for example, a "marginal" wave in a thin channel, then pockets of unburned gas and unreactive transverse waves were possible in all mixtures. Edwards observed similar pockets experimentally and numerical simulations [87] showed that these pockets were associated with "peninsulas of cooler material". Oran et al. [87] recognized that the delayed burning of these pockets could play an important role in detonation propagation and the near-limit behavior of detonations.

Gamezo et al. [88] conclude on the basis of numerical simulations that the mechanism by which the pockets are consumed also varied with the activation energy of the mixture. They propose that in low-activation energy mixtures, the reaction was by auto-ignition after shock compression, while in high activation energy mixtures, the pockets were consumed by heat and mass exchange with neighboring hot gases. Radulescu et al. [83,82,13] have examined low pressure methane–oxygen mixtures in narrow channels from both a computational and experimental point of view. They find evidence of extensive unburned pockets and argue that diffusive burning must occur relatively close to the reaction front (within $4\Delta_i$ for near CJ waves and $6\Delta_i$ in the case of marginal waves propagating at 80% of the CJ speed) in order for the waves to be self-sustaining. In the case of simulations, this occurs through numerical diffusion. In experiments, the mixing produced by Kelvin–Helmholtz and Richtmyer–Meshkov instabilities plays an important role in enabling diffusive mixing and combustion [89,90] to occur relatively rapidly downstream of the main reaction region.

The influence of mixture type on detonation diffraction was examined by Moen et al. [53,91] and Desbordes [92]. The critical tube diameter for weakly unstable mixtures was as large as 40 cell sizes λ while for strongly unstable mixtures, the critical tube diameter on the order of 10–15 λ. More recently, Pintgen [66]

has examined the details of detonation diffraction in weakly and strongly unstable mixtures and quantified the differences in the centerline velocity decay rate for the subcritical cases. The most striking differences between the mixtures occur in the subcritical and critical regimes, for which the detonation fails to transition into the unconfined half-space. For the H_2-O_2-Ar mixture, the velocity on the center line was found to decay significantly slower than for the H_2-N_2O mixture. In case of a H_2-O_2-Ar mixture, it was evident from simultaneous schlieren-fluorescence images that the reaction front was coupled to the lead shock front up to 2.3 tube diameters from the exit plane. For a H_2-N_2O mixture, the reaction front velocity decreased to 60% of the corresponding Chapman–Jouguet value at 1.1 tube diameters from the tube exit plane. Analysis of processes in the reaction zone region of the diffracting wave [66] indicates that there are significant differences in critical decay time and activation energy between the two mixtures.

The behavior of detonations in impervious and absorbing wall tubes depends crucially on mixture type. In smooth tubes with hard walls, the limiting (failure) diameter and velocity deficits are smaller for strongly unstable as compared to weakly unstable mixture types [91]. Dupre et al. [93] and also Teodorczyk and Lee [94] examined the limiting conditions for propagation in tubes with a section of acoustic absorbing surfaces; Radulescu and Lee [95] extended these studies over a wide range of mixture types. Radulescu and Lee find that regular mixtures have a critical failure diameter of 11 λ and propagated up to 100 λ before failure. Strongly unstable mixtures have a critical failure diameter of 4 λ and only propagate a short distance, less than 10 λ, prior to failure. They argue that the results imply that transverse waves are essential for the propagation of strongly unstable waves while playing a relatively small role in the propagation of weakly unstable waves. They propose that in the strongly unstable cases, the transverse wave collisions and resulting turbulent mixing play a key role in propagation and that failure occurs due to the damping of the transverse waves. On the other hand, in weakly unstable cases, they propose that the main shock front is responsible for the reaction, and failure mechanism is related to the curvature of the wavefront and the very slow decoupling processes associated with curvature evolution.

Finally, Kuznetsov et al. [96] examined transition-to-detonation run-up distance. They find that for weakly unstable mixtures, the DDT scale length had to be at least 40 λ while for strongly unstable mixtures it was only 7 λ.

Summary The conclusion from all of these studies is that the extent of instability has to be considered in formulating experiments on and modeling detonation waves. There is no universal reaction zone structure or set of correlations to macroscopic behavior. There are trends that are useful for engineering purposes, but from a scientific viewpoint, different considerations are

needed for treating the extremes in behavior. In particular, there is very strong evidence that in the strongly unstable cases, some fraction of the reactants pass through the main reaction zone without reacting, and if a detonation is to propagate persistently and not fail outright, turbulent mixing and diffusive reaction must take place not too far downstream of the main front.

3 Simulating Detonation Fronts

Examining Fig. 1a, we note that the characteristic propagation distance in typical laboratory experiments is 1–10 m, while the reaction zone shown in Figs. 1c and d exhibits significant spatial gradients on the order of 1–10 μm. Despite the widespread availability of software for adaptive mesh refinement, this range of 10^7 in length scales obviously poses a significant issue (see the discussions in [83,97–100]) for accurate direct numerical simulation of the reactive, viscous flow with detailed chemical reaction kinetics. Other considerations include the storage requirements for detailed chemical reaction mechanisms with 50–500 individual species needed for typical hydrocarbon fuels [101], the three-dimensional nature of the coherent structures and turbulent flow in the reaction zone, and the challenge of carrying out high-order simulations needed for turbulence modeling and simultaneously capturing shock waves [102].

The majority of numerical simulations have been carried out using the Euler (inviscid) equations formulated in conservative form and a simplified chemical reaction kinetic model in either one [86,103–109,12,110–112] or two [48,61,83,88,100,112–125] dimensions. The most common reaction kinetics model is the irreversible one-step Arrhenius rate with simple depletion although two- [113,126,79], three- [127,128], four- [123], and five-step[125] models have been used to mimic features of realistic mechanisms such as chain-branching, competition for radicals, and explosion limit or "cross-over" effects.

A small number of simulations have been carried out with detailed chemical reaction mechanisms using the Euler (inviscid) formulation for hydrogen–oxygen–argon mixtures in one- [129–132], two- [133–136], and three-dimensions [137] and also, for ethylene–oxygen mixtures [138] in one-dimension. The most ambitious and realistic studies have been the three-dimensional simulations of the Navier–Stokes equations by Oran et al. [139] using a one-step irreversible reaction and adaptive mesh refinement. Manifold approximation methods have been explored [130,140,141], and reduced kinetic mechanisms have been specifically developed for detonation conditions in hydrogen [142] and hydrocarbon fuels [143–146]. Data from high-pressure shock tube experiments [147] are vital for validating mechanisms over the full range of thermodynamic conditions encountered in detonations.

3.1 Chain-branching reactions and the competitions for radicals

The reaction that takes place behind the leading shock front (Fig. 1c and d) is a coupled chain-branching, thermal explosion in which exponential growth of radical species, recombination reactions forming products and releasing thermal energy, and competing reaction pathways for intermediates all occur simultaneously. All of these effects are included automatically when a full detailed chemistry model is used for simulation. However, these models are not practical for large-scale multidimensional simulations nor suitable for analytical computations with approximate methods such as activation energy asymptotic analysis. For this reason, substantial efforts have gone into developing ad hoc models with pseudo-species that mimic some portion of the actual chemical processes.

Ad hoc reaction models contain a number of adjustable constants which, for engineering applications, need to be selected to mimic the behavior of an actual combustible mixture. One way to go about this is to match the induction time, energy release time, and effective activation energy computed on the basis of detailed chemical kinetics for a range of thermodynamic conditions that will be encountered in the detonation simulation. This will assure that the key parameters E/RT and Δ_i/Δ_e will be correctly approximated. Computations [125,148] of these reaction zone parameters for hydrogen and a representative hydrocarbon, ethane, are shown in Fig. 6. Note that the ratio of time scales τ_i/τ_e is shown rather than the ratio of length scales.

In mixtures with hydrogen as fuel, the competition for H atoms produces a broad zone of high effective activation energy in the temperature–pressure plane, Fig. 6a. The peak of the activation energy appears coincident with the classical extended second limit [149–153] as specified by reaction rate ratios. Although a change in reaction mechanism and effective activation energy is observed when crossing this zone, experimental measurements [154,155] indicate detonations are possible beyond the extended limit. A reduced reaction model must take this effect into account since significant variations in activation energy may occur within the reaction zone of an unstable detonation due to the oscillation of the postshock state across the extended second limit.

For mixtures with ethane as fuel, simulations of near-stoichiometric mixtures with air show that the reduced activation energy is a slowly varying function for a wide range of temperature–pressure conditions, Fig. 6c. Apparently, a relatively simple reaction model of type proposed by Varatharajan et al. [156] would be adequate in these cases since the induction and energy release times have a very smooth and simple dependence on the thermodynamic state. There are certainly competing reaction pathways for many of the intermediate species but apparently no single bottleneck that creates the sharp ridge in E/RT that

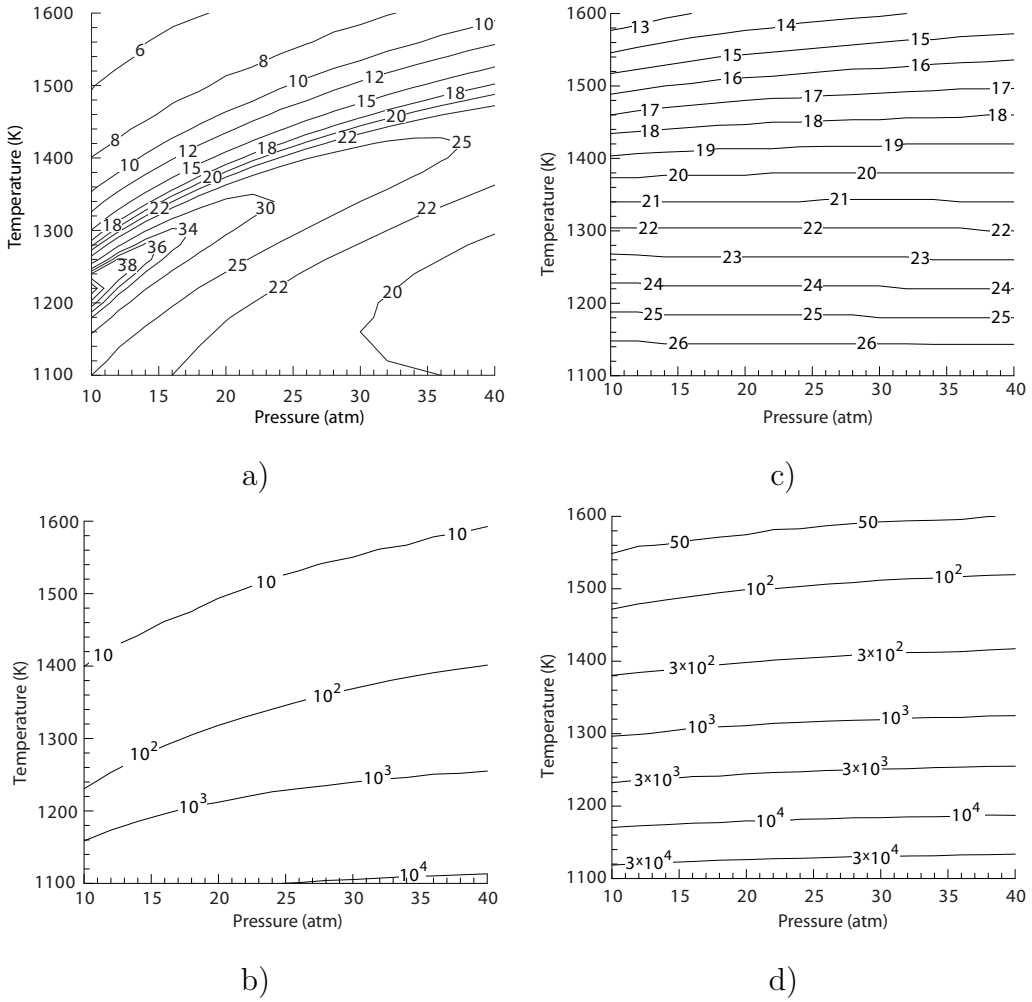

Fig. 6. a) and c) Reduced effective activation energy $\theta = E/RT$, b) and d) reaction zone shape parameter τ_i/τ_e for stoichiometric a) and b) hydrogen-air and c) and d) ethane-air computed using detailed reaction mechanisms and the constant volume explosion model [148].

is shown in Fig. 6a.

For both mixtures, the ratio τ_i/τ_e becomes quite large at low temperature since the induction time τ_i is a relatively strong function of the temperature due to the dependence on the branching chain reaction rates and the energy release time τ_e is a relatively weak function of temperature since the recombination processes are strongly exothermic and the rates are relatively independent of temperature.

Liang et al. [125] used the approach described above to calibrate a five-step, four-species model that simulated hydrogen combustion. Numerical simulations of propagating detonations were performed for the two mixture conditions shown in Fig. 7a. Case 1 (Fig. 7b) has relatively constant reaction zone parameters with modest values of E/RT and τ_i/τ_e and the solution is clearly

of the weakly unstable type. Case 2 (Fig. 7c) has reaction zone parameters that change drastically as the postshock state oscillates and crosses the "ridge line" corresponding to the cross-over region in Fig. 7a. As a consequence, Case 2 appears to be of the strongly unstable type of mixture with pockets of unreacted mixture downstream of the main reaction zone and a highly irregular reaction front and leading shock.

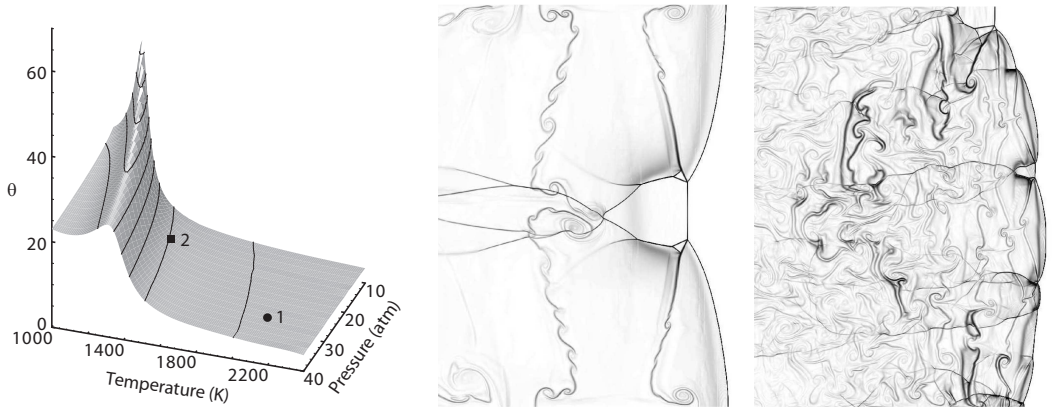

a) b) c)

Fig. 7. a) Reduced effective activation energy $\theta = E/RT$ and vN points (CJ speed) for cases 1 and 2, [125]. Numerical schlieren images from simulations based on the five-step model: b) Case 1, weakly unstable, $7 < E/RT < 4$, $1.5 < \tau_i/\tau_e < 0.9$ for $0.85 < U/U_{CJ} < 1$. c) Case 2, strongly unstable, $29 < E/RT < 10$, $33 < \tau_i/\tau_e < 1.3$ for $0.85 < U/U_{CJ} < 1$.

3.2 Statistical Analysis of Highly-Unstable Detonations

Conventional turbulent flow analysis is based on applying statistical methods to data and modeling fluctuations in flow quantities as random variables described by probability distributions. The notion of applying Reynolds decomposition to detonations was proposed by White [14] in 1961 shortly after the discovery of detonation instability. At the time, developing realistic closure relationships for the Reynolds-averaged equations was not attempted. Today, we still lack sufficiently fast and high-enough resolution diagnostics to measure the fluctuations experimentally but we are in position to make some progress using data from simulations. Radulescu et al. [83] have considered this issue in some detail and analyzed the output of two-dimensional numerical simulations of unstable detonation waves using Favre averaging to separate the flow into mean and fluctuating components. Their analysis shows that the effective sonic surface is located at 20 Δ_i (weakly unstable) to 60 Δ_i (highly unstable) from the mean shock front. They show that a subtle balance between mean flow and fluctuations determines the location of the effective sonic surface. The mechanical fluctuation intensity was found to decay from 30% just behind the

leading shock to less than 1% at the location of the effective sonic plane.

Statistical analysis can also be used as a diagnostic tool for comparing the average and fluctuating properties of unstable detonation simulations. As an example, we show analysis of the data of Liang et al. [125] discussed above. Time series data of the lead shock speed and reaction zone thickness at three points in the channel for Cases 1 and 2 are shown in Fig. 8. The time series were then post-processed to obtain the relative frequency distributions, Fig. 9. Finally, the joint relative frequency distribution of reaction zone length and shock speed was computed and compared with the deterministic result based on a quasi-steady reaction zone, Fig. 10.

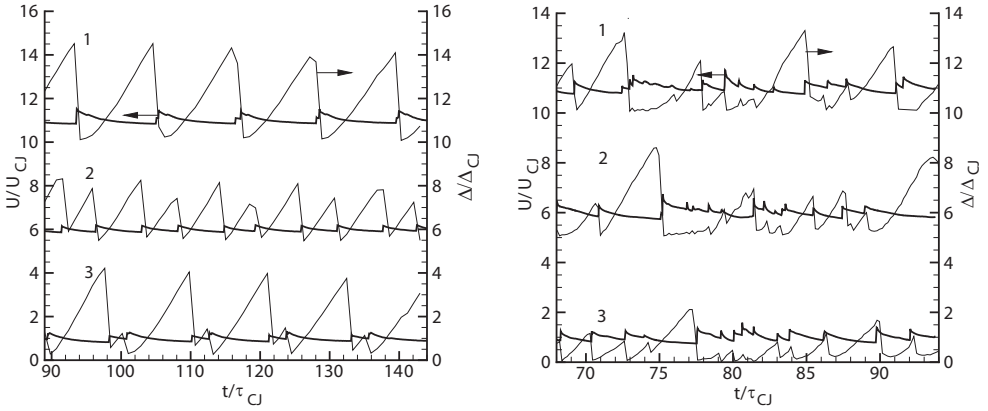

Fig. 8. Time series of normalized lead shock speed and reaction zone thickness at three locations: 1 - $H/2$, 2 - $H/3$, 3 - $H/6$ where H is the channel height. The time series for locations 1 and 2 have been displaced vertically for clarity. a) Case 1. b) Case 2.

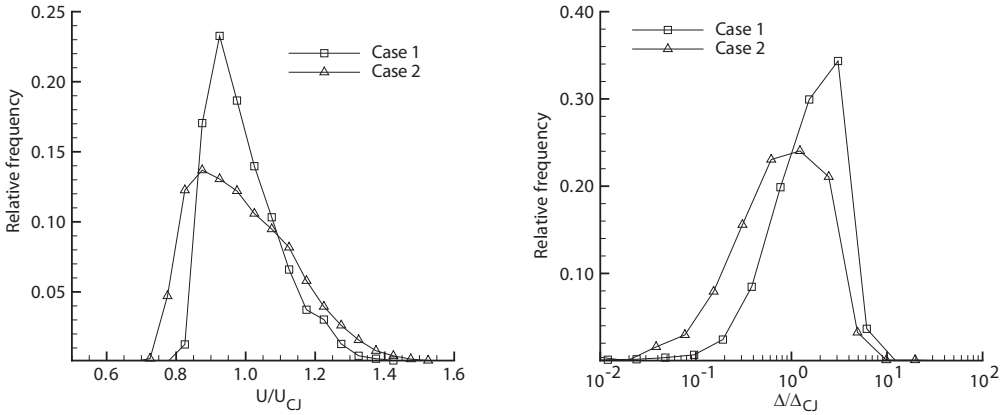

Fig. 9. Relative frequency distributions. a) Lead shock speed b) Reaction zone length.

The time series in Fig. 8 clearly show the irregular nature of Case 2 as com-

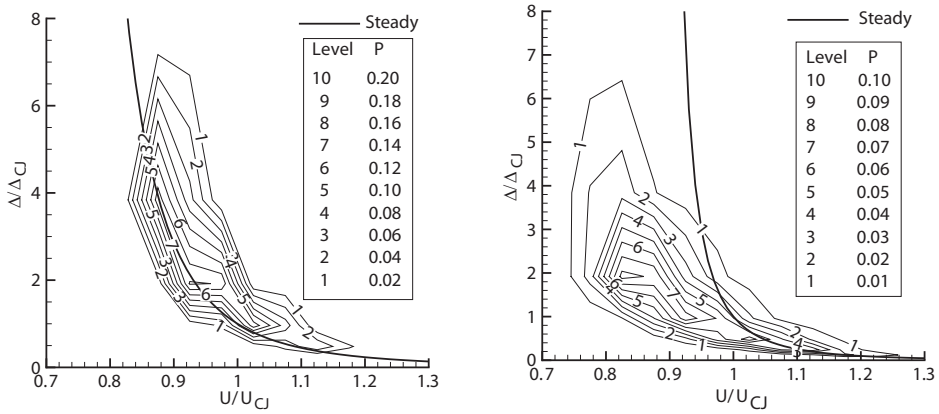

a) b)

Fig. 10. Joint frequency distributions of normalized reaction zone length and shock speed. a) Case 1 b) Case 2.

pared to the regular periodicity of Case 1. The frequency distributions in Fig. 9a for shock speed are skewed with the most probable value below CJ and the spread in speeds larger for Case 2 than Case 1. The speed frequency distributions are in qualitative agreement with the analysis by Austin [32] of the data of Eckett [130] and the more recent study by Radulescu et al. [83]. The frequency distributions in Fig. 9b for reaction zone length are skewed in the opposite direction to velocity but this is reasonable given the inverse relation between shock speed and reaction zone length. The real value of the statistical analysis is realized in Fig. 10 in which we compare the joint distributions with the quasi-steady relationship $\Delta(U)$ obtained from the constant-volume explosion model. Case 1 shown in Fig. 10a has a joint distribution function that is sharply peaked and well aligned with the quasi-steady solution. Case 2 shown in Fig. 10b only follows the quasi-steady distribution at sufficiently high shock speeds, and at low speeds, there is a large discrepancy between the joint distribution and the quasi-steady result. The results for Case 2 are in agreement with the computations [32,85] using the critical decay rate model and photographic measurements of wave speed for highly-unstable waves. The results for Case 1 are in agreement with the previous critical decay rate analysis [35] of experiments and simulations with weakly unstable waves. We conclude that the reaction zone must be treated as fully unsteady for highly-unstable waves except in the highest speed portions of the wavefront. On the other hand, the reaction zone can be treated as quasi-steady for all portions of the weakly unstable waves.

3.3 Dynamical Systems Approach

The instability of detonations has also been examined from a dynamical systems point of view [81,109,157]. Linear stability theory [74,75,158–160] predicts that with increasing activation energy E (all other parameters being fixed) the ZND structure will become unstable to small perturbations and an increasing number of unstable modes will be accessible with further increases in E. Numerical simulations of the nonlinear evolution of unstable modes [109] using activation energy for a one-step reaction as a control parameter show a sequence of period-doublings and ultimately transition to chaos following the appearance of a "period three" bifurcation. These computations were repeated [81] using the two-step model of Short and Sharpe [79] and qualitatively similar results were obtained. Henrick et al. [157] used the shock change equation to avoid errors caused by capturing the lead shock front and a high-order numerical method. They investigated even higher activation energies and show that the system ultimately transitions from chaos back to a nonlinear limit cycle with a modest number of modes. It is not clear what the implications are for computing two- and three-dimensional flows, but clearly some caution is in order beyond the usual tests of numerical sensibility.

Summary We conclude that significant advances have been made in detonation simulation in the last decade. Computation of detonations in one dimension now appears to be well established on the basis of the Euler equations, and it is possible to handle fairly complex chemical reaction mechanisms and even remove some of the shock-capturing errors with special treatment of the leading shock. Simulation of detonation in two- and three-dimensions with resolved reaction zones is becoming easier with the availability of robust software for adaptive mesh refinement and complex boundaries. However, progress in sub-grid scale modeling for reaction zones has lagged behind similar efforts for low-speed turbulent combustion, and a clear need for this has been identified [83] for highly-unstable detonation propagation. Scientific investigations will continue to make incremental progress as growth in computing capability enables more realistic models, in addition to the spatial and temporal resolution needed to do direct simulation of the turbulent flow in the reaction zone. Application to engineering problems [161] of detonation initiation and propagation are feasible but careful attention has to be given to validation and scaling.

4 Conclusions

There is no single paradigm for detonation front structure but a range of behavior that depends on mixture type, boundary, and initial conditions. In spite of this variability, there are clear trends in the combustion regimes that can be observed as the mixture parameters are varied. We presented experimental and numerical evidence for the transition between these regimes using systematic variations of the composition of the reactants. Ideal reaction zone models and ideas from instability theory were used to suggest figures of merit for describing the instability regime. We have shown the usefulness of statistically characterizing the wave speed fluctuations and demonstrated the role of unsteadiness through quantitative statistical analysis.

Central to further progress is the elucidation of the high-speed turbulent combustion processes within the reaction front and development of models for engineering and scientific simulation of compressible turbulent flows. In common with other turbulent reacting flows, the challenge is to use limited resources to obtain sufficient spatial and temporal resolution for meaningful measurements and simulation. In the case of simulation, there are further difficulties with the realism of physical and chemical models. The primary experimental needs are high-resolution, quantitative measurements of chemical species and flow fields within the reaction zone that can be used for model development and validation. The key challenge, as in low speed flows, is in the statistical characterization of a turbulent flow field. The primary theoretical and simulation need is for a sub-grid-scale model of turbulent combustion that will enable quantitative engineering predictions of macroscopic detonation behavior.

Acknowledgments

I have been privileged to work at Caltech with an extraordinarily talented group of young researchers who deserve all the credit for the results shown here. The statistical analysis that is shown in Figs. 8-10 was carried out by Z. Liang. Financial support was provided by Caltech and grants from Los Alamos National Laboratory, US Department of Energy, and the Office of Naval Research. I thank S. Kao and J. Karnesky for their assistance in preparing this manuscript.

This paper is dedicated to John H.S. Lee of McGill University who first introduced me to the intricacies of the gas detonation phenomenon and has had the greatest influence on my thinking about detonations over the past three decades. For myself and many others engaged in the scientific study of detonations, John is a primary source of knowledge, encouragement, provocative

ideas, and a staunch advocate of the central role of turbulence in unstable detonation waves.

References

[1] M. Bertherlot, P. Vielle, *Ann. de Phys. et Chim.* 28 (v) (1881) 289.

[2] E. Mallard, H. L. Le Chatelier, *Annales des Mines* 8 (iv) (1881) 274–618.

[3] G. D. Roy, S. M. Frolov, A. A. Borisov, D. W. Netzer, *Prog. Energy Combust. Sci.* 30 (6) (2004) 545–672.

[4] T. V. Bazhenova, V. V. Golub, *Combust. Explos. Shock Waves* 39 (4) (2003) 365–381.

[5] D. W. Stamps, M. Berman, *Nucl. Sci. Eng.* 109 (1) (1991) 39–48.

[6] J. E. Shepherd, in: *ASME Pressure Vessels and Piping Conference.*, ASME, 2006, Paper PVP2006-ICPVT11-93670, July 23-27 2006 Vancouver BC Canada.

[7] G. Ciccarelli, S. Dorofeev, *Prog. Energy Combust. Sci.* 34 (4) (2008) 499–550.

[8] S. Gordon, B. J. McBride, *Computer Program for Calculation of Complex Chemical Equilibrium Compositions and Applications. I. Analysis*, Reference Publication RP-1311, NASA (1994).

[9] Z. C. Owens, D. W. Mattison, E. A. Barbour, C. I. Morris, R. K. Hanson, *Proc. Combust. Inst.* 30 (2005) 2791–2798.

[10] D. W. Mattison, M. A. Oehischlaeger, C. I. Morris, Z. C. Owens, E. A. Barbour, J. B. Jeffries, R. K. Hanson, *Proc. Combust. Inst.* 30 (2005) 2799–2807.

[11] M. Radulescu, R. Hanson, *J. Prop. Power* 21 (2) (2005) 274–285.

[12] A. R. Kasimov, D. S. Stewart, *Phys. Fluids* 16 (10) (2004) 3566–3578.

[13] J. H. S. Lee, M. I. Radulescu, *Combust. Explos. Shock Waves* 41 (6) (2005) 745–765.

[14] D. R. White, *Phys. Fluids* 4 (4) (1961) 465–480.

[15] Y. N. Denisov, Y. K. Troshin, *Dokl. Akad. Nauk SSSR* 125 (1) (1959) 110–113.

[16] B. V. Voitsekhovskii, V. V. Mitrofanov, M. E. Topchian, *Struktura fronta detonastii i gaza*, 1963, Translation: Rep. FTD-MT-64-527, Foreign Technology Division, Wright-Patterson A.F.B., Ohio, 1966.

[17] R. I. Soloukhin, *Combust. Flame* 9 (1) (1965) 51–58.

[18] G. L. Schott, *Phys. Fluids* 8 (5) (1965) 850–865.

[19] D. H. Edwards, *Proc. Combust. Inst.* 12 (1969) 819–828.

[20] R. A. Strehlow, *Astron. Acta* 15 (5) (1970) 345–357.

[21] A. K. Oppenheim, *Introduction to the Gasdynamics of Explosions*, Springer, 1970, International Center for Mechanical Sciences, Courses and Lectures No. 48, Udine, Italy.

[22] J. H. S. Lee, *The Detonation Phenomenon*, Cambridge University Press, 2008.

[23] Y. B. Zel'dovich, *J. Exp. Theo. Phys.* 10 (1940) 542–568, available in translation as NACA TM 1261 (1950).

[24] W. Döring, *Ann. Phys.* 43 (1943) 421–436.

[25] J. von Neumann, in: A. J. Taub (Ed.), John von Neumann, collected works, Vol. 6, MacMillan, 1942, pp. 203–218.

[26] W. Fickett, W. C. Davis, *Detonation*, University of California Press, Berkeley, CA, 1979.

[27] D. S. Stewart, A. R. Kasimov, *J. Prop. Power* 22 (6) (2006) 1230–1244.

[28] A. A. Vasil'ev, *J. Prop. Power* 22 (6) (2006) 1245–1260.

[29] Y. B. Zel'dovich, *J. Exp. Theo. Phys.* 12 (1) (1942) 389.

[30] G. I. Taylor, *Proc. R. Soc. Lond.* A 200 (1950) 235–247.

[31] R. Akbar, *Mach Reflection of Gaseous Detonations*, Ph.D. thesis, Rensselaer Polytechnic Institute, Troy, New York (August 1997).

[32] J. Austin, *The Role of Instability in Gaseous Detonation*, Ph.D. thesis, California Institute of Technology, Pasadena, California (Jun. 2003).

[33] S. Jackson, J. Austin, J. E. Shepherd, *AIAA J.* 44 (10) (2006) 2422–2425.

[34] F. Pintgen, J. M. Austin, J. E. Shepherd, in: G. D. Roy, S. M. Frolov, R. J. Santoro, S. A. Tsyganov (Eds.), Confined Detonations and Pulse Detonation Engines, Torus Press, Moscow, 2003, pp. 105–116.

[35] F. Pintgen, C. A. Eckett, J. Austin, J. E. Shepherd, *Combust. Flame* 133 (3) (2003) 211–229.

[36] J. M. Austin, F. Pintgen, J. E. Shepherd, *Proc. Combust. Inst.* 30 (2005) 1849–1857.

[37] I. O. Moen, J. W. Funk, S. A. Ward, G. M. Rude, P. A. Thibault, Vol. 94 of *Prog. Astronaut. Aeronaut.*, 1984, pp. 55–79.

[38] J. H. S. Lee, *Ann. Rev. Fluid Mech.* 16 (1984) 311–336.

[39] R. Knystautas, C. Guirao, J. H. Lee, A. Sulmistras, Vol. 94 of *Prog. Astronaut. Aeronaut.*, 1984, pp. 23–37.

[40] W. B. Benedick, C. M. Guirao, R. Knystautas, J. H. Lee, Vol. 106 of *Prog. Astronaut. Aeronaut.*, 1986, pp. 181–202.

[41] S. Dorofeev, V. P. Sidorov, M. S. Kuznetzov, I. D. Matsukov, V. I. Alekseev, *Shock Waves* 10 (2) (2000) 137–149.

[42] M. Kaneshige, J. E. Shepherd, *Detonation Database*, Tech. Rep. FM97-8, Graduate Aeronautical Laboratories, California Institute of Technology, available at `http://www.galcit.caltech.edu/detn_db/html/` (1997).

[43] J. M. Austin, J. E. Shepherd, *Combust. Flame* 132 (1-2) (2003) 73–90.

[44] D. W. Stamps, S. E. Slezak, S. R. Tieszen, *Combust. Flame* 144 (1-2) (2006) 289–298.

[45] G. Ciccarelli, J. Card, *AIAA J.* 44 (2) (2006) 362–367.

[46] C. K. Westbrook, P. A. Urtiew, *Proc. Combust. Inst.* 19 (1982) 615–623.

[47] A. A. Vasil'ev, *Combust. Explos. Shock Waves* 34 (1) (1998) 72–76.

[48] A. I. Gavrikov, A. A. Efimenko, S. B. Dorofeev, *Combust. Flame* 120 (1-2) (2000) 19–33.

[49] A. Y. Kusharin, G. L. Agafonov, O. E. Popov, B. E. Gelfand, *Combust. Sci. Technol.* 135 (1-6) (1998) 85–98.

[50] N. Lamoureux, C. E. Paillard, *Shock Waves* 13 (1) (2003) 57–68.

[51] H. D. Ng, Y. Ju, J. H. S. Lee, *Intl. J. Hydrogen Energy* 32 (1) (2007) 93–99.

[52] M. O. Sturtzer, N. Lamoureux, C. Matignon, D. Desbordes, H. N. Presles, *Shock Waves* 14 (1-2) (2005) 45–51.

[53] J. E. Shepherd, I. O. Moen, S. B. Murray, P. A. Thibault, *Proc. Combust. Inst.* 21 (1986) 1649–1658.

[54] J. J. Lee, D. Garinis, D. L. Frost, J. H. S. Lee, R. Knystautas, *Shock Waves* 5 (3) (1995) 169–174.

[55] O. V. Achasov, O. G. Penyazkov, *Shock Waves* 11 (4) (2002) 297–308.

[56] B. B. Botros, H. D. Ng, Y. Zhu, Y. Ju, J. H. S. Lee, *Combust. Flame* 151 (4) (2007) 573–580.

[57] C. Guo, G. Thomas, J. Li, D. Zhang, *Shock Waves* 11 (5) (2002) 353–359.

[58] C. M. Guo, C. J. Wang, S. L. Xu, H. H. Zhang, *Combust. Flame* 148 (3) (2007) 89–99.

[59] Z. W. Huang, M. H. Lefebvre, P. J. Van Tiggelen, *Shock Waves* 10 (2) (2000) 119–125.

[60] K. Ishii, M. Kojima, *Shock Waves* 17 (1-2) (2007) 95–102.

[61] B. Khasainov, H. N. Presles, D. Desbordes, P. Demontis, P. Vidal, *Shock Waves* 14 (3) (2005) 187–192.

[62] M. Kuznetsov, G. Ciccarelli, S. Dorofeev, V. Alekseev, Y. Yankin, T. H. Kim, *Shock Waves* 12 (3) (2002) 215–220.

[63] S. Ohyagi, T. Obara, S. Hoshi, P. Cai, T. Yoshihashi, *Shock Waves* 12 (3) (2002) 221–226.

[64] T. Slungaard, T. Engebretsen, O. K. Sonju, *Shock Waves* 12 (4) (2003) 301–308.

[65] F. Pintgen, *Laser-Optical Visualization of Detonation Structures*, Diplom Arbeit, TU München, Graduate Aeronautical Laboratories, California Institute of Technology (Dec. 2000).

[66] F. Pintgen, *Detonation Diffraction in Mixtures with Various Degrees of Regularity*, Ph.D. thesis, California Institute of Technology (Dec. 2004).

[67] D. H. Edwards, G. Hooper, R. J. Meddins, *Astron. Acta* 17 (4-5) (1972) 475–485.

[68] T. Nagaishi, K. Yoneda, T. Hikita, *Combust. Flame* 16 (1) (1971) 35–38.

[69] R. A. Strehlow, A. J. Crooker, *Acta Astronautica* 1 (3-4) (1974) 303–315.

[70] V. A. Subbotin, *Fiz. Goreniya Vzryva* 11 (3) (1975) 486–491.

[71] R. A. Strehlow, *Astron. Acta* 14 (5) (1969) 539–548.

[72] J. C. Libouton, A. Jacques, P. J. Van Tiggelen, *Actes du Colloque International Berthelot-Vieille-Mallard-Le Chatelier* 2 (1981) 437–442, Bordeaux, France.

[73] V. Y. Ul'yanitskii, *Fiz. Goreniya Vzryva* 17 (2) (1981) 127–133.

[74] H. I. Lee, D. S. Stewart, *J. Fluid Mech.* 216 (1990) 103–132.

[75] M. Short, D. S. Stewart, *J. Fluid Mech.* 368 (1998) 229–262.

[76] P. Howe, R. Frey, G. Melani, *Combust. Sci. Technol.* 14 (1976) 63–74.

[77] V. J. Manzhalevi, V. A. Subbottin, *Combust. Explos. Shock Waves* 12 (6) (1977) 819–825.

[78] M. Short, *J. Fluid Mech.* 430 (2001) 381–400.

[79] M. Short, G. J. Sharpe, *Combust. Theor. Model.* 7 (2) (2003) 401–416.

[80] H. D. Ng, *The effect of chemical reaction kinetics on the structure of gaseous detonations*, Ph.D. thesis, McGill University, Montreal Quebec Canada (June 2005).

[81] H. D. Ng, M. I. Radulescu, A. J. Higgins, N. Nikiforakis, J. H. S. Lee, *Combust. Theor. Model.* 9 (3) (2005) 385–401.

[82] M. I. Radulescu, G. J. Sharpe, J. H. S. Lee, C. B. Kiyanda, A. J. Higgins, R. K. Hanson, *Proc. Combust. Inst.* 30 (2005) 1859–1867.

[83] M. I. Radulescu, G. J. Sharpe, C. K. Law, J. H. S. Lee, *J. Fluid Mech.* 580 (2007) 31–81.

[84] F. Pintgen, J. E. Shepherd, in: G. D. Roy, A. A. Berlin, S. M. Frolov, J. E. Shepherd, S. A. Tsyganov (Eds.), Proc. of the Intl. Coll. Appl. Det. Prop., Torus Press, Moscow, 2004, pp. 23–28.

[85] J. M. Austin, F. Pintgen, J. E. Shepherd, AIAA Paper 2005-1170 (2005).

[86] C. A. Eckett, J. J. Quirk, J. E. Shepherd, *J. Fluid Mech.* 421 (2000) 147–183.

[87] E. S. Oran, T. R. Young, J. P. Boris, J. P. Picone, D. H. Edwards, *Proc. Combust. Inst.* 19 (1982) 573–582.

[88] V. N. Gamezo, D. Desbordes, E. Oran, *Combust. Flame* 116 (1-2) (1999) 154–165.

[89] L. Massa, J. M. Austin, T. L. Jackson, *J. Fluid Mech.* 586 (2007) 205–248.

[90] M. Arienti, J. E. Shepherd, *The Role of Diffusion in Irregular Detonations*, the 4th Joint Meeting of the US Sections of the Combustion Institute, Philadelphia, PA, March 20-23 (2005).

[91] I. O. Moen, A. Sulmistras, G. O. Thomas, D. Bjerketvedt, P. A. Thibault, Vol. 106 of *Prog. Astronaut. Aeronaut.*, 1986, pp. 220–243.

[92] D. Desbordes, C. Guerraud, L. Hamada, H. N. Presles, Vol. 153 of *Prog. Astronaut. Aeronaut.*, 1993, pp. 347–359.

[93] G. Dupre, O. Peraldi, J. H. Lee, R. Knystautas, Vol. 114 of *Prog. Astronaut. Aeronaut.*, 1988, pp. 248–263.

[94] A. Teodorczyk, J. H. S. Lee, *Shock Waves* 4 (1995) 225–236.

[95] M. I. Radulescu, J. H. S. Lee, *Combust. Flame* 131 (1-2) (2002) 29–46.

[96] M. S. Kuznetsov, V. I. Alekseev, S. B. Dorofeev, *Shock Waves* 10 (3) (2000) 217–223.

[97] P. Hwang, R. P. Fedkiw, B. Merriman, T. D. Aslam, A. R. Karagozian, S. J. Osher, *Combust. Theor. Model.* 4 (3) (2000) 217–240.

[98] J. M. Powers, S. Paolucci, *AIAA J.* 43 (5) (2005) 1088–1099.

[99] J. M. Powers, *J. Prop. Power* 22 (6) (2006) 1217–1229.

[100] G. J. Sharpe, J. J. Quirk, *Combust. Theor. Model.* 12 (1) (2008) 1–21.

[101] C. K. Westbrook, Y. Mizobuchi, T. J. Poinsot, P. J. Smith, J. Warnatz, *Proc. Combust. Inst.* 30 (2005) 125–157.

[102] D. J. Hill, D. I. Pullin, *J. Phys. Chem.* 194 (2) (2004) 435–450.

[103] A. L. Sanchez, M. Carretero, P. Clavin, F. A. Williams, *Phys. Fluids* 13 (3) (2001) 776–792.

[104] L. He, J. H. S. Lee, *Phys. Fluids* 7 (5) (1995) 1151–1158.

[105] Y. Daimon, A. Matsuo, *Phys. Fluids* 15 (1) (2003) 112–122.

[106] M. Short, D. Y. Wang, *Combust. Theor. Model.* 5 (3) (2001) 343–352.

[107] G. J. Sharpe, *J. Fluid Mech.* 447 (2001) 31–51.

[108] K. Mazaheri, S. A. Hashemi, *Combust. Sci. Technol.* 179 (8) (2007) 1701–1736.

[109] H. D. Ng, A. J. Higgins, C. B. Kiyanda, M. I. Radulescu, J. H. S. Lee, K. R. Bates, N. Nikiforakis, *Combust. Theor. Model.* 9 (1) (2005) 159–170.

[110] H. D. Ng, B. B. Botros, J. Chao, J. M. Yang, N. Nikiforakis, J. H. S. Lee, *Shock Waves* 15 (5) (2006) 341–352.

[111] H. D. Ng, J. H. S. Lee, *J. Fluid Mech.* 476 (2003) 179–211.

[112] S. D. Watt, G. J. Sharpe, *J. Fluid Mech.* 522 (2005) 329–356.

[113] E. S. Oran, J. P. Boris, T. Young, M. Flanigan, T. Burks, M. Picone, *Proc. Combust. Inst.* 18 (1981) 1641–1649.

[114] S. Taki, T. Fujiwara, *Proc. Combust. Inst.* 18 (1981) 1671–1681.

[115] A. Bourlioux, A. Madja, *Combust. Flame* 90 (3-4) (1992) 211–229.

[116] D. A. Jones, G. Kemister, E. S. Oran, M. Sichel, *Shock Waves* 6 (3) (1996) 119–129.

[117] E. G. Pantow, M. Fischer, T. Kratzel, *Shock Waves* 6 (3) (1996) 119–129.

[118] D. N. Williams, L. Bauwens, E. S. Oran, *Shock Waves* 6 (2) (1996) 93–110.

[119] V. N. Gamezo, D. Desbordes, E. S. Oran, *Shock Waves* 9 (1) (1999) 11–17.

[120] A. K. Kapila, D. W. Schwendeman, J. J. Quirk, T. Hawa, *Combust. Theor. Model.* 6 (4) (2002) 553–594.

[121] A. M. Khokhlov, J. M. Austin, F. Pintgen, J. E. Shepherd, AIAA Paper No. 2004-0792 (2004).

[122] M. Arienti, J. E. Shepherd, *J. Fluid Mech.* 529 (2005) 117–146.

[123] Z. Liang, L. Bauwens, *Shock Waves* 15 (3-4) (2006) 247–257.

[124] Z. Liang, L. Bauwens, *Combust. Theor. Model.* 9 (3-4) (2006) 93–112.

[125] Z. Liang, S. Browne, R. Deiterding, J. E. Shepherd, *Proc. Combust. Inst.* 31 (2007) 2445–2453.

[126] G. J. Sharpe, *Phys. Fluids* 14 (12) (2002) 4372–4388.

[127] M. Short, A. K. Kapila, J. J. Quirk, *Phil. Trans. R. Soc. Lond.* 357 (1764) (1999) 3621–3637.

[128] G. J. Sharpe, N. Maflahi, *J. Fluid Mech.* 566 (2006) 163–194.

[129] Y. Daimon, A. Matsuo, *Phys. Fluids* 19 (11) (2007) 116101.

[130] C. Eckett, *Numerical and Analytical Studies of the Dynamics of Gaseous Detonations*, Ph.D. thesis, California Institute of Technology (2000).

[131] S. Y. Yungster, K. Radhakrishnan, *Combust. Theor. Model.* 8 (4) (2004) 745–770.

[132] B. Wang, H. He, S. T. J. Yu, *AIAA J.* 43 (10) (2005) 2157–2169.

[133] E. S. Oran, J. W. Weber, Jr., E. I. Stefaniw, M. H. Lefebvre, J. D. Anderson, Jr., *Combust. and Flame* 113 (1-2) (1998) 147–163.

[134] X. Y. Hu, D. L. Zhang, B. C. Khoo, Z. L. Jiang, *Combust. Theor. Model.* 8 (2) (2004) 339–359.

[135] X. Y. Hu, D. L. Zhang, B. C. Khoo, Z. L. Jiang, *Shock Waves* 11 (1-2) (2004) 475–480.

[136] R. Deiterding, in: *High Performance Computing And Communications, Proceedings*, no. 3726 in Lecture Notes In Computer Science, Springer, 2005, pp. 916–927.

[137] N. Tsuboi, K. Eto, A. K. Hayashi, *Combust. Flame* 149 (1-2) (2007) 144–161.

[138] S. Yungster, K. Radhakrishnan, *Shock Waves* 14 (1-2) (2005) 61–72.

[139] E. S. Oran, V. N. Gamezo, *Combust. Flame* 148 (1-2) (2007) 4–47.

[140] S. Singh, Y. Rastigejev, S. Paolucci, J. M. Powers, *Combust. Theor. Model.* 5 (2) (2001) 163–184.

[141] G. Dong, B. C. Fan, Y. L. Chen, *Combust. Theor. Model.* 11 (5) (2007) 823–837.

[142] T. F. Lu, C. K. Law, Y. G. Ju, *J. Prop. Power* 19 (5) (2003) 901–907.

[143] M. V. Petrova, F. A. Williams, *Combust. Sci. Technol.* 179 (5) (2007) 961–986.

[144] B. Varatharajan, F. A. Williams, *J. Prop. Power* 18 (2) (2002) 344–351.

[145] B. Varatharajan, F. A. Williams, *J. Prop. Power* 18 (2) (2002) 352–362.

[146] B. Varatharajan, F. A. Williams, *Combust. Flame* 124 (4) (2001) 624–645.

[147] E. L. Petersen, R. K. Hanson, *J. Prop. Power* 15 (4) (1999) 591–600.

[148] S. Browne, Z. Liang, J. E. Shepherd, *Detailed and Simplified Chemical Reaction Mechanisms for Detonation Simulation*, paper 05F-21 - Presented at the Fall 2005 Western States Section of the Combustion Institute, Stanford University, Oct. 17-18, 2005 (2005).

[149] V. V. Voevodesky, R. I. Soloukhin, *Proc. Combust. Inst.* 10 (1965) 279–283.

[150] W. C. Gardiner, C. B. Wakefield, *Astron. Acta* 15 (1970) 399–409.

[151] J. W. Meyer, A. K. Oppenheim, *Proc. Combust. Inst.* 13 (1970) 1153–1164.

[152] J. W. Meyer, A. K. Oppenheim, *Combust. Flame* 17 (1) (1971) 65–68.

[153] E. S. Oran, J. P. Boris, *Combust. Flame* 48 (2) (1982) 135–148.

[154] S. R. Tieszen, M. P. Sherman, W. B. Benedick, J. E. Shepherd, R. Knystautas, J. H. S. Lee, Vol. 106 of *Prog. Astronaut. Aeronaut.*, 1986, pp. 205–219.

[155] J. Shepherd, Vol. 106 of *Progress in Astronautics and Aeronautics*, AIAA, 1986, pp. 263–293.

[156] B. Varatharajan, M. Petrova, F. A. Williams, V. Tangirala, *Proc. Combust. Inst.* 30 (2005) 1869–1877.

[157] A. K. Henrick, T. D. Aslam, J. M. Powers, *J. Comput. Phys.* 213 (1) (2006) 311–329.

[158] J. J. Erpenbeck, *Phys. Fluids* 7 (5) (1964) 684–696.

[159] A. R. Kasimov, D. S. Stewart, *J. Fluid Mech.* 466 (2002) 179–203.

[160] A. Tumin, *AIAA J.* 45 (9) (2007) 2356–2359.

[161] V. E. Tangirala, A. J. Dean, P. F. Pinard, B. Varatharajan, *Proc. Combust. Inst.* 30 (2005) 2817–2824.